Journal of ASTM International, June 2005, Vol. 2, No. 6
Paper ID JAI12441
Available online at www.astm.org

A. Glendening,[1] *D. A. Koss,*[1] *A. T. Motta,*[2] *O. N. Pierron,*[1] *and R. S. Daum*[3]

Failure of Hydrided Zircaloy-4 Under Equal-Biaxial and Plane-Strain Tensile Deformation

ABSTRACT: The fracture behavior of unirradiated Zircaloy-4 containing either solid hydride blisters or hydrided rims has been examined for the contrasting conditions of equal-biaxial and plane-strain tensile deformation at three temperatures (25°, 300°, and 375°C). Cold-worked and stress-relieved Zircaloy-4 sheet containing hydride blisters shows nearly identical failure strains in equal-biaxial and plane-strain tensile deformation for a wide range of blister or rim depths. In all cases, failure strains decrease rapidly with increasing hydride blister or rim thickness, especially in the ≤100 μm range. Test temperature has a significant effect on ductility with failure strains at 300° and 375°C being much greater than at room temperature. The results indicate that the ductility of material containing hydride rims/blisters greater than ≈ 30–40 μm deep is limited by crack growth, which occurs in a mode I manner at 25°C but in a mixed mode I/II manner at ≥300°C (and at higher failure strain levels).

KEYWORDS: Zircaloy-4, mechanical testing, hydride rim, hydride blisters, biaxial deformation, reactivity initiated accident

Introduction

The normal operation of nuclear fuel in light water reactors results in degradation of the mechanical behavior of the fuel cladding due to a combination of oxidation, hydriding, and radiation damage. These degradation processes have been increasing steadily due to longer fuel residence times (higher burnup) and more severe fuel duty cycles. These higher levels of cladding oxidation and hydrogen pickup accumulated by the cladding may increase the likelihood of cladding failure during design-basis accidents. One such postulated design-basis accident is the reactivity-initiated accident (RIA). An RIA may be caused by the ejection of a control rod from the core, which causes a rapid insertion of reactivity and thermal energy in the fuel [2] and an accompanying increase in fuel temperature. The resulting fuel expansion and release of fission gases force the cladding into multiaxial tension.

Thus, the survivability of cladding when subject to an RIA after long reactor exposures depends on a combination of: (i) the mechanics of loading, (ii) the temperature at which the loading occurs, *and* (iii) the degree of material degradation during the preceding reactor exposure [2,3]. While radiation-induced changes to mechanical properties, such as hardening, appear to saturate at relatively low damage levels [4,5], material degradation caused by hydriding continues to increase steadily. As a result, the level, nature, and distribution of hydrides are major factors in determining the survivability of high burnup cladding during an RIA. Because of the heat flux present in the reactor, hydride precipitates often form preferentially near the

Manuscript received 31 March 2004; accepted for publication 17 November 2004; published June 2005. Presented at ASTM Symposium on Zirconium in the Nuclear Industry: Fourteenth International Symposium on 13–17 June 2004 in Stockholm, Sweden; B. Kammenzind and P. Rudling, Guest Editors.
[1] Dept. Materials Sci. and Eng., Penn State University, University Park, PA 16802.
[2] Dept. of Mech and Nucl. Eng., Penn State University, University Park, PA 16802.
[3] Argonne National Laboratory, Argonne, IL 60439.

outer (cooler) surface of the cladding. Eventually a continuous layer/rim containing a high concentration of discrete hydride particles may develop. Hydride blisters can also form, usually under conditions where oxide spallation occurs, creating a local temperature gradient. The blisters are usually lens shaped (typically a few mm in major dimension) and consist of a very high hydride concentration or a solid hydride [1].

As illustrated in Fig. 1, the mechanics of loading are such that the cladding deformation path ranges from near plane-strain hoop tensile deformation (as is the case for a closed-end, thin-wall tube subject to gas pressure) to equal-biaxial tensile deformation (as expected to be the case for cladding well bonded to isotropically expanding fuel). Thus, the mechanics of loading dictate a tensile strain path bracketed by plane-strain tensile deformation ($\varepsilon_2 = 0$) and equal-biaxial tensile deformation in which the two in-plane strain increments are equal ($\varepsilon_1 = \varepsilon_2$), as shown in Fig. 1. [We note that that plastic deformation of the thin wall cladding tube occurs under a condition of *plane stress* in the through-thickness direction; the *plane-strain* condition applies to the deformation path in the plane of the cladding tube, such as along its axis.]

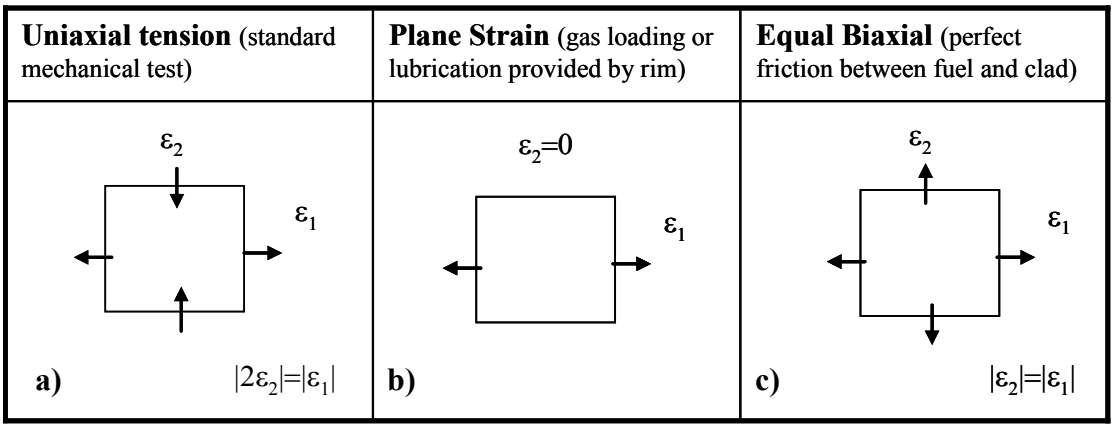

FIG. 1—*A schematic illustration of a range of possible strain paths for thin-wall cladding deforming under a plane-stress condition ($\sigma_3 = 0$).*

While the influence of multiaxial stress states and strain paths on the failure of ductile metals is well known, much less is known about the role of multi-axial loading on the hydrogen embrittlement of Zircaloy-4. Several studies have examined aspects of plane-strain failure behavior of hydrided Zircaloy-4 using the burst behavior of hydrided tubes [1,6,7] and notched specimens [8–12]. The most direct study of the influence of multiaxial strain path on the hydrogen embrittlement of hydrided Zircaloy is a room-temperature study based on *recrystallized* Zircaloy-4 sheet that contained a *uniform* distribution of hydride precipitates throughout the sheet thickness [13]. As discussed later, the results obtained in that study indicate a large decrease of ductility with both increasing hydrogen content and increasing degree of biaxiality of strain path. However, the sensitivity of Zircaloy ductility to multiaxial strain path *and* hydride distributions typical of high burnup cladding, such as when hydrides are concentrated in a rim or a blister near the cladding surface [11,12], has not been determined.

This study addresses the fracture behavior of Zircaloy-4 sheet containing *solid hydride blisters*, subjected to an *equal-biaxial tensile deformation path*, and fractured at either 25°, 300°, or 375°C. As such, this research contrasts previous studies where either uniaxial or plane-strain deformation paths were used. The equal-biaxial behavior will also be compared to that under *plane-strain tensile deformation* of Zircaloy-4 in the form of both sheet and cladding tube

containing either hydride blisters or rims of dense hydride particles. In so doing, this study is intended to bound the fracture behavior of cladding subject to a likely range of stress states/strain paths imposed on the cladding during an RIA event. While plane-strain ductility is becoming more common as a basis for a failure criterion for cladding undergoing an RIA, this study also provides insight into the validity of such a criterion if the cladding is forced into a deformation path with a significant biaxial component.

This study utilizes flat, cold-worked and stress-relieved (CWSR) Zircaloy-4 sheet, which has a crystallographic texture (and plastic anisotropy) similar to that of as-fabricated Zircaloy-4 cladding tubes. To induce equal-biaxial tensile deformation as in Fig. 1*c without* bending, we developed a new test procedure that relies on punch-stretch testing using a "flat-bottom" punch. These results are contrasted to the behavior of hydrided Zircaloy in the form of double-edge notched specimens (both sheet and cladding tube) in which the biaxial tension induces a near plane-strain tensile deformation path within the gauge section.

Experimental Procedure

Materials

For experimental ease, most of this study is based on the behavior of hydrogen-charged Zircaloy-4 sheet (obtained from Teledyne Wah-Chang). This is the same material used in a previous study [12]. The cold-worked, stress-relieved sheet (CWSR) was 0.64 mm thick and had an elongated grain structure with grains approximately 10 μm long and roughly 1–2 μm thick. As described elsewhere [12], the sheet had strong crystallographic texture. Importantly, the Kearns factors [15] of this CWSR sheet (f_N = 0.59, f_R = 0.05, and f_T = 0.31 in the normal, longitudinal/rolling, and transverse directions of the sheet, respectively) are similar to those reported for unirradiated CWSR Zircaloy-4 cladding tubes (0.58, 0.10, and 0.32, respectively) [16] if the hoop direction of the tube corresponds to the orientation transverse to the rolling direction of the sheet. Therefore, the texture of the Zircaloy-4 sheets used in this study is similar to the typical texture of Zircaloy-4 cladding tubes, i.e., the basal planes tend to align with their poles inclined approximately ± 30º away from the normal of the tube surface and oriented toward the transverse direction. [17]

The tensile properties of the Zircaloy-4 sheet are also described in more detail elsewhere [18]. Compared to the tensile behavior of Zircaloy-4 cladding in the hoop direction, the sheet is about ≈120 MPa softer at room temperature and ≈100 MPa softer at 300°C when tested transverse to the rolling direction [19]. Both materials have similar plastic anisotropy values: for the sheet, the plastic anisotropy parameter R' (R' = $\varepsilon_{width}/\varepsilon_{thickness}$, where ε_{width} and $\varepsilon_{thickness}$ are the width and thickness strains during uniform deformation in a tensile test) is such that R' = 2.2 at 25°C and R' = 1.6 at 300°C. The strain-hardening exponent of the sheet used in this study (n = $d\ln\sigma/d\ln\varepsilon$ = 0.01 at 25°C to 0.03 at 300°C) is significantly smaller than that of standard cladding (n ≅ 0.06 at 300°C) [19]. In fact, the strain hardening behavior of this sheet material is similar to that of irradiated cladding [20]. As will be described later, a comparison of the sheet ductility with that of tubing under plane-strain conditions will show the sheet to be more ductile. This means that the *absolute* values of the strains measured here for sheet material should not be used to predict failure in cladding tubes.

A few results will be presented based on the behavior of CWSR Zircaloy-4 cladding tubes charged with hydrogen such that a dense layer of hydrides or *hydride rim* was present near the outer surface of the cladding. Details of that material are reported elsewhere [11].

Hydrogen Charging

Hydrogen charging of the Zircaloy-4 sheet was performed by gas charging at 400°C using a Ni "window" whose geometry controlled the dimensions of the hydride layer (i.e., 3 mm diameter blister or continuous layer [12]). The Ni coating was formed by vapor-depositing Ni in a vacuum chamber of total pressure of $\approx 1 \times 10^{-3}$ Pa. Hydrogen charging was performed by exposing the Ni-coated specimen to a gas mixture of 12.5 %H_2/Argon at 2.1×10^7 Pa pressure for charging times ranging from 10–90 min at 400°C (this is well below the stress-relief temperature used in annealing the sheet; no microstructure change was apparent). After charging, the specimen was cooled to room temperature at a rate of ≈ 40°C/min. The equal biaxial specimens were subsequently annealed at 300°C for 4 h to "stabilize" the hydride structure against any further changes during the 300°C tests.

The hydride microstructure after charging was examined using both light microscopy and scanning electron microscopy (SEM). Specimens were prepared for examination by mechanical grinding ranging from 240–1200 grit. The specimens were then etched up to 5 s with a 10 part-HNO_3-20 part-H_2O-1 part-HF solution to reveal the hydrides. The depth of the 3 mm diameter blister was roughly a linear function of the charging time, and cross-section metallography showed that the blister diameter corresponded to the Ni coating diameter. In addition, some hydrogen diffused throughout the sheet thickness to form discrete hydrides in the "substrate" region just beneath the hydride blister. Analysis of the hydrogen concentration beneath the hydride blisters show hydrogen contents in the range of 300–400 wt. ppm as the hydride rim increased in depth from 50 μm to >100 μm [12].

Mechanical Testing

In earlier studies [19] we simulated plane-strain loading with a double edge-notched tensile specimen designed to introduce a biaxial stress state in the specimen center such that near plane-strain tensile deformation is achieved (i.e., the minor strain component in the plane of the sheet is near zero, Fig. 1*b*). For the Zircaloy-4 sheet material, the specimens used were 25.4 mm wide specimens (≈ 76 mm long) with two 4.75 mm diameter notches, each of which was 6.35 mm deep. In the case of the cladding tube specimens, the double edge-notch ring stretch specimens were used as described elsewhere [11,19]. In both cases, failure initiated in the specimen center, where the deformation path is near the plane-strain condition.

To impose equal-biaxial tensile deformation for this study, we utilized a "flat bottom" punch stretch procedure in which sheet specimens are deformed under a balanced, equal-biaxial tensile deformation path [21–23]. In contrast with the hemispherical punch-stretch technique used in a previous study of hydrogen embrittlement of Zircaloy under biaxial tension [13] (where the specimens were subjected to a combination of bending and stretching), this technique does not cause bending during deformation. As shown in Fig. 2*a*, the punch, which has a circular cross-section, has a slightly concave bottom surface that allows the central section of the specimen to remain flat and free from contact with the punch during deformation, thus also avoiding friction effects. In this study, the steel punch had a diameter of 25.4 mm and was configured so that the central 10 mm of the specimen remained flat to the failure strains during stretching. The surrounding die had a 27 mm inner diameter and a 77 mm outer diameter; six bolts were used to provide hold-down pressure to avoid draw-in of the 58 mm diameter sheet.

Success of the in-plane, equal-biaxial stretch test requires the use of a second sheet with a central hole. The second sheet, which acts as a spacer and has the shape of a "washer," is located

between the punch and the Zircaloy specimen, and it allows load transfer to the central region of the sheet specimen. Without the washer, the "friction hill" between the punch and specimen causes failure of the specimen as it contacts the punch at the punch radius. In our tests, the "washer" was a 0.6-mm thick alpha brass disk, with an 8 mm diameter hole in the center. As shown in Fig. 2*a*, the washer and specimen were clamped together in the die. To further promote load transfer to the central region of the sheet, a lubricant (molybdenum disulfide) was used in the brass-punch interface. Figure 2*b* shows the radial distribution of in-plane true plastic strain measurements performed after deformation of a specimen. The circular shape obtained for the strains verifies that the strain path is equal biaxial tensile deformation in the plane of the sheet over the central 8 mm of the flat central region of the specimens. Because of the plastic anisotropy of the material, an equal-biaxial strain path will be similar to but not identical with an equal biaxial stress state path. For the case where there is tight bonding between fuel and cladding during an RIA, the deformation of the material should be displacement-controlled, in which case equal-biaxial tension is the appropriate strain path for the cladding.

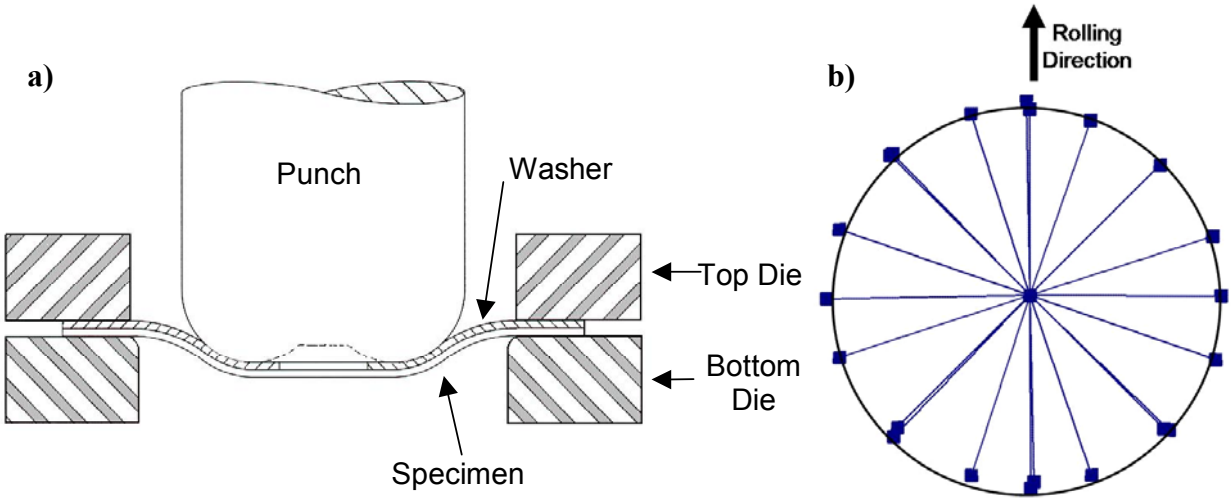

FIG. 2—*(*a*) A schematic of the punch stretch apparatus and (*b*) a representation of in-plane true strain values ($(\varepsilon)_{ave}$ = 0.125) as a function of radial orientation and as determined over the central 10 mm of the punch-stretch specimen.*

The hydrided Zircaloy-4 sheet was tested at three temperatures: 25°, 300°C, or 375°C; a few ring-stretch tests on hydrided cladding tube material were also performed at 375°C using a procedure described elsewhere [11,19]. For the plane-strain tests of sheet material, the orientation of the tensile axis was chosen to be in the long transverse direction of the sheet (normal to the rolling direction) in order to obtain deformation behavior similar to that of unirradiated Zircaloy-4 cladding tube when tested in the hoop direction. For experimental ease, tests were performed under the quasi-static strain rate of $\cong 10^{-3}$/s, compared to strain rates of 10^{-1}/s to 1/s or higher anticipated in RIA conditions [14]. Recent room temperature results indicate no strain-rate dependence of failure strains of cold worked and unirradiated Zircaloy-2 cladding tubes with over 330 wt. ppm hydrogen [14]; as described later, this level of hydrogen corresponds well to the hydrogen concentration within the cold worked Zircaloy-4 substrate beneath the hydrogen blister in our study. We note that the present quasi-static test conditions, failure occurs in $\leq$200 s from crack initiation within the blister, a time too short for delayed hydride cracking [24,25].

Failure strains for the equal-biaxial tests were measured using two distinct methods. The first method was based on thickness measurements at locations roughly 0.4–0.5 mm from the fracture surface within the blisters. This distance was chosen to avoid the localized deformation that occurred very close (except at very thin blister depths, ≤0.2 mm) to the fracture surface due (as will be discussed later) to crack growth. Using a measuring microscope at 15× to view the fractured sheet in profile, we determined the *local* thickness strain $(\varepsilon_3)_{local}$ at the onset of fracture using the relationship $(\varepsilon_3)_{local} = ln(t_f/t_o)$, where t_f and t_o are the final and initial thicknesses, respectively. Assuming constant volume during equal-biaxial deformation, the maximum principal *tensile* strain at failure initiation is thus $(\varepsilon_f)_{local} = -(1/2)\ (\varepsilon_3)_{local}$. For a 0.6 mm-thickness sheet containing small cracks, distances of 0.5 mm or greater from the fracture surface avoid any localized thickness reduction due to the plasticity associated with the fracture process. Thus, as is common in studies of sheet metal failure [23], the strain values determined in this manner indicate the strain level at the onset of failure. A similar procedure was used for plane-strain testing to determine a $(\varepsilon_f)_{local}$ value [12].

A second failure strain determination was also employed. In the equal-biaxial test case, eight microhardness indentations were spaced equally in the matrix around the perimeter of the 3 mm hydride blister. The spacings between groups of the two indentations whose connecting line passed through the center of the blister were determined before and after specimen failure in a manner similar to that shown in Fig. 2, except that the displacement across fracture surface was subtracted from the final spacing between the two indentations. As a result, four "in-plane" true strain values were determined across the failed blister in each test. These four *far-field failure strain values* $(\varepsilon_f)_{far}$ indicate the accumulated plastic strain averaged over a 3+ mm scale across and immediately adjacent to the blister just prior to failure. The experimental determinations of $(\varepsilon_f)_{far}$ were generally quite consistent in values. Also, as will be shown later, in most cases $(\varepsilon_f)_{far} \cong (\varepsilon_f)_{local}$. The exception was at very small blister depths where extensive local necking caused the local failure strain value to be somewhat greater than the far-field failure strain value. Far-field strains at failure were also determined for the plane-strain tests of Zircaloy-4 sheet containing hydride blisters. Those $(\varepsilon_f)_{far}$-values, which agree closely with the $(\varepsilon_f)_{local}$-values reported elsewhere [12], were based on the initial and final blister dimension, omitting the displacements across the fracture surface. The procedure for determining the $(\varepsilon_f)_{far}$-values in the ring stretch tests relies on measuring distances between microhardness indentations and is described elsewhere [11,19,26]. A similar microhardness indentation procedure was used to determine $(\varepsilon_f)_{far}$-values for the flat sheet specimens containing a solid hydride rim.

Results and Discussion

Hydride Microstructure

For the equal-biaxial specimens, the hydrogen gas charging procedure produced hydride blisters beneath the Ni coating, in the form of solid hydrides with depths within ± 5 % of reported values, as shown in Fig. 3. These 3 mm diameter blisters had depths ranging from ≈25–150 μm. Within the substrate material beneath the hydride blister, individual hydride precipitates form as shown in the lightly etched microstructure shown in Fig. 3. As shown in the following sections, these hydride precipitates tend to be aligned in the plane of the sheet, similarly to the circumferential hydride microstructures in Zircaloy cladding tube. Previous results from six different plane-strain specimens with hydride depths ranging from 50–175 μm show that the H

concentration within the ligament increases from approximately 300 wt. ppm for the 50 μm blister depth, to approximately 400 wt. ppm for blisters with depths >100 μm. Comparison of hydride precipitate microstructures between the equal-biaxial specimens and the plane-strain test specimens indicate similar hydride characteristics within the substrate region, and thus we assume similar hydrogen concentrations in the substrate.

It is worth noting that the microstructure shown in Fig. 3 is similar to microstructures observed in Zircaloy-4 cladding after extended in-reactor operation. Specifically, solid hydride layers ≈ 50 μm and a concentration of discrete, circumferential hydride precipitates (hydride rim) were also present in irradiated Zircaloy-4 cladding tubes irradiated to a fuel burnup of 67 GWd/t (see Fig. 3 of Ref. [12]).

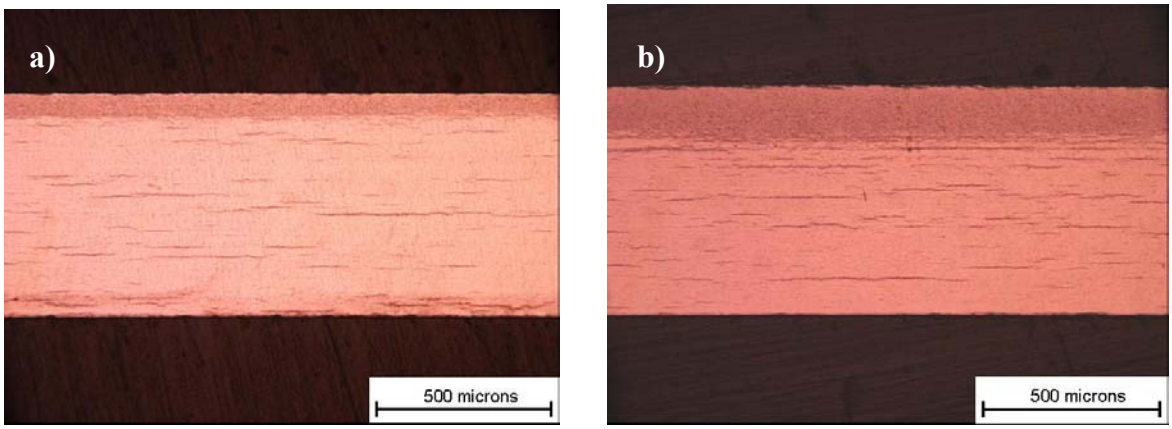

FIG. 3—*Optical micrographs showing a cross-section of Zircaloy-4 sheet containing hydride blisters that are (*a*) 50 μm deep and (*b*) 150 μm deep. Note the hydride precipitates in the substrate beneath the blisters. The horizontal direction is parallel to the rolling direction.*

The Influence of Blister Depth and Strain Path on Failure

Cladding loading during an RIA involves multi-axial stresses such that the resulting strain path is expected to range between plane-strain tension and equal biaxial tension, as depicted in Fig. 1. For the case of *plane-strain* tensile deformation, previous research has shown that the thicknesses of both continuous hydride rims and hydride blisters have a strong influence on the failure of Zircaloy-4 [11,12,27]. Specifically, increasing the thickness of the hydride rim/blister decreases the ductility, especially for blister/rim depths of greater than about 100 μm [11,12].

Similar to plane-strain deformation failure behavior described above [11,12,25], Fig. 4 shows that, under *equal-biaxial* tensile deformation, both *far-field* and *local* failure strains decrease rapidly with increasing hydride blister depth, with most of the decrease occurring at blister depths of less than about 100 μm. Both definitions of the failure strain show similar behavior. At least for this Zircaloy-4 sheet, a significant level of ductility ($(\varepsilon_1)_{ebt} \cong 0.04$) is retained at 25°C, even for blisters of depths ≅ 140 μm. Also as in the plane-strain case, the hydrided Zircaloy is significantly more ductile at both 300° and 375°C than at 25°C, as measured by the maximum principal strain at failure. Thus, at 300°C, the residual ductility at large blister depths is even greater, being of the order of $(\varepsilon_1)_{ebt} \approx 0.08$.

Relatively little is known about the influence of multiaxial deformation path on failure of hydrided Zircaloy. The single previous related study was confined to recrystallized Zircaloy-4

sheet containing a uniform distribution of hydride precipitates throughout the sheet thickness and tested solely at room temperature [13]. Those results indicate a large decrease of ductility with increasing degree of biaxiality of tensile deformation, especially at elevated hydrogen contents. For example, comparing the equal-biaxial fracture strains $(\varepsilon_1)_{ebt}$ to those obtained under plane-strain tensile deformation $(\varepsilon_1)_{p\varepsilon}$, that study showed similar ductilities at low hydrogen contents ($\cong$ 150 wt ppm where $(\varepsilon_1)_{ebt} \approx (\varepsilon_1)_{p\varepsilon}$), but at the 615 ppm hydrogen level, the equal biaxial ductility was much less: $(\varepsilon_1)_{ebt} \approx 0.4(\varepsilon_1)_{p\varepsilon}$. The authors of that study [13] attributed the strain path effect to the ability of randomly oriented hydride precipitates, many along grain boundaries, to promote fracture along a multi-directional path characteristic of equal-biaxial tensile failure (see Fig. 6). However, the aligned hydride precipitate microstructure within the substrate beneath the hydride blister in the present CWSR material (Fig. 3) is not only much different than that in recrystallized Zircaloy, but it also suggests an increased fracture resistance under equal-biaxial tension.

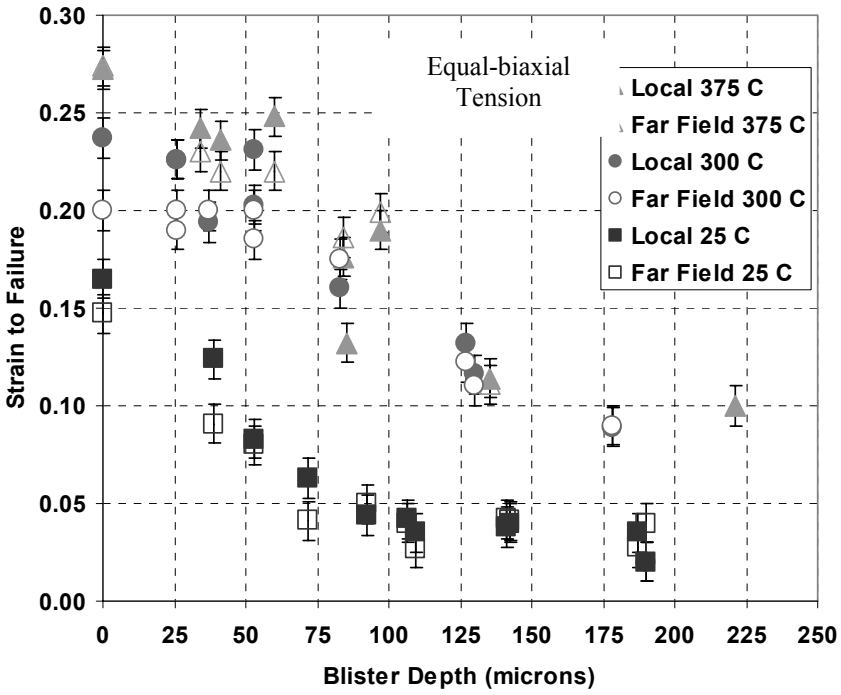

FIG. 4—*The dependence of failure strain on hydride blister thickness for equal biaxial tensile deformation strain path of Zircaloy-4 sheet containing 3 mm diameter blisters and tested at either 25°C, 300°C, or 375°C. See text for definitions of local and far-field failure strains.*

To compare the degree of embrittlement under equal-biaxial tension with that in plane-strain tensile deformation, Fig. 5 presents the *far-field* failure strain behavior for both conditions. The most striking feature of Fig. 5 is the similarity of failure strain values between the two strain paths to failure. A similar strain path comparison based on *local* failure strains also shows nearly identical behavior to that shown in Fig. 5, with perhaps even closer agreement between the two sets of failure-strain values. Thus, the strain-path effect on ductility seen previously in recrystallized Zircaloy [13] is not reproduced, most likely due to the differences in hydride microstructures within the bulk of the material (specifically, the difficulty of the fracture path to

link the aligned hydride particles within the substrate beneath the blister). Based on this data, we conclude that, with the possible exception of thin blister behavior at 25°C, the failure of CWSR Zircaloy-4 containing hydride blisters is *insensitive* to strain path in the range of plane-strain to equal-biaxial tensile deformation. An important implication of Fig. 5 is that *current procedures to determine failure strains under plane-strain tensile deformation are likely to obtain minimum principal strain values that represent a lower bound to cladding ductility, i.e., plane-strain testing can be used as a lower bound for RIA testing because equal biaxial tensile deformation is not more penalizing to cladding ductility than plane strain tensile deformation*.

The Fracture Process

Previous results indicate that the hydride blisters are brittle even at 400°C [12] so that at strains near the yield strain of the Zircaloy substrate, the blisters crack. As shown in Fig. 6*a* and 6*c*, fracture of the brittle hydride blister in equal-biaxial-tensile deformation creates the characteristic "mud-cake" crack pattern in the plane of the sheet as the cracks form normal to the multi-directional orientations of the maximum principal stresses (i.e., $\sigma_1 \approx \sigma_2$) in the plane of the sheet. Measurements of the magnitudes of the crack opening displacements within cracked blisters shown in Fig. 6 confirm the brittle fracture within the hydride blisters even at 375°C. Occasionally, the fracture initiation site within the hydride blister is quite obvious, such as in the example shown in Fig. 7.

In contrast to the equal-biaxial case, plane-strain tensile deformation initiates relatively well aligned, planar cracks within the blister; as expected, the cracks are oriented normal to the maximum principal stress σ_1 (Figs. 6*b* and 6*d*). An analysis of test specimens such as shown in Fig. 6 indicates that the crack spacing increases with blister thickness and with test temperature, as previously observed [12].

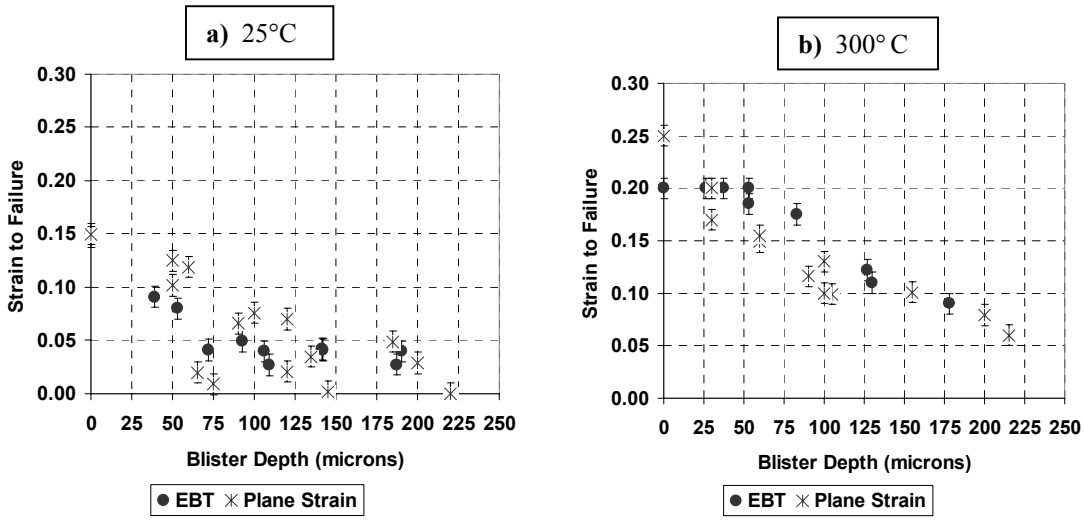

FIG. 5—*A comparison between the far-field failure strains in equal biaxial tensile deformation (EBT) with those in plane-strain tensile deformation for Zircaloy-4 sheet containing hydride blisters of different depths and tested at (*a*) 25°C and (*b*) 300°C.*

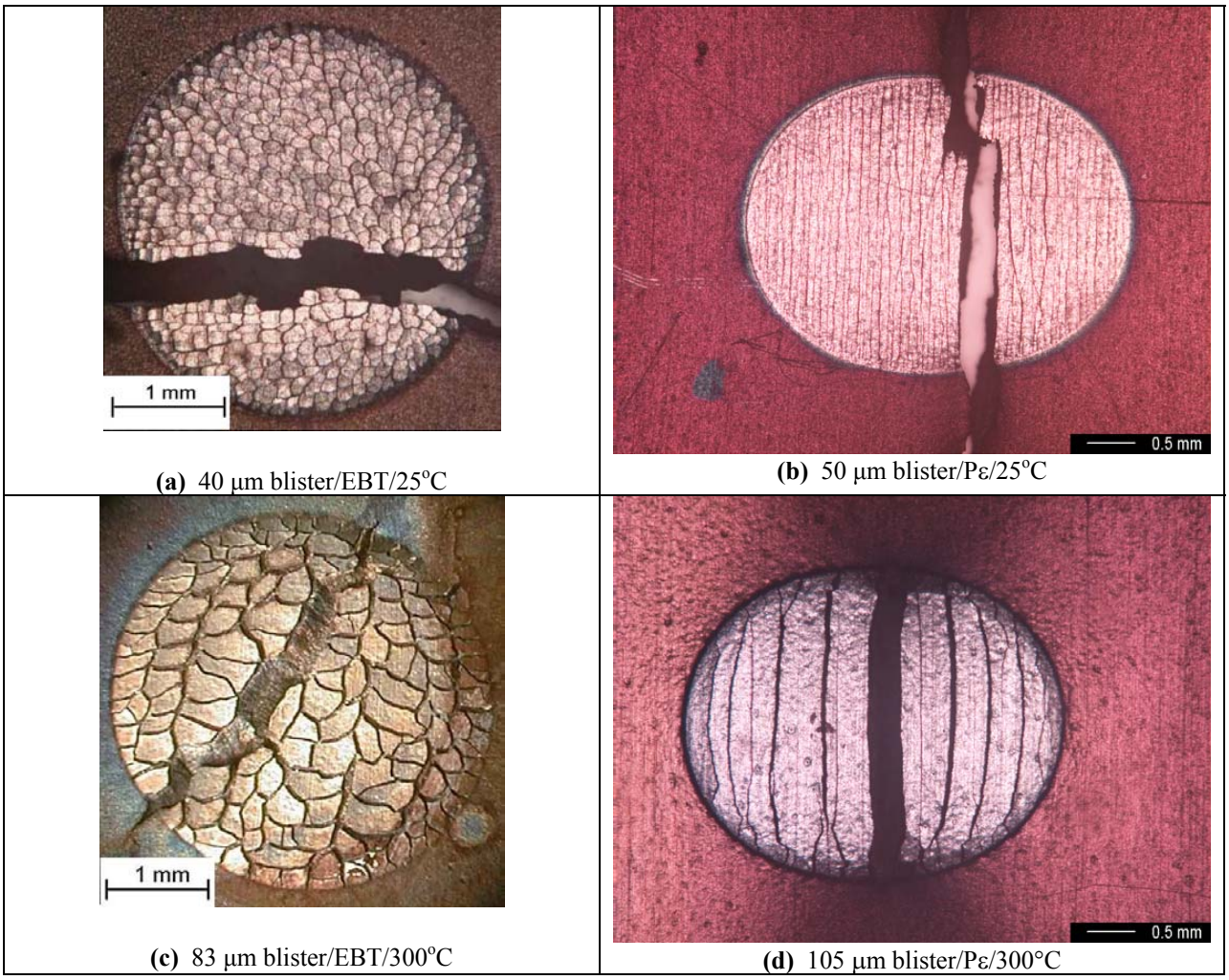

(a) 40 μm blister/EBT/25°C

(b) 50 μm blister/Pε/25°C

(c) 83 μm blister/EBT/300°C

(d) 105 μm blister/Pε/300°C

FIG. 6—*Optical micrographs showing a comparison of crack patterns within hydride blisters in Zircaloy-4 sheet failed in either equal-biaxial (EBT) or plane-strain tensile deformation (Pε). Test temperatures and hydride blister depths are indicated. The horizontal direction is transverse to the rolling direction in the plane-strain tests; no systematic orientation dependence was detected in the equal-biaxial case. Note that* (a) *and* (c) *have different magnifications than* (b) *and* (d)*, which are after Ref. [12].*

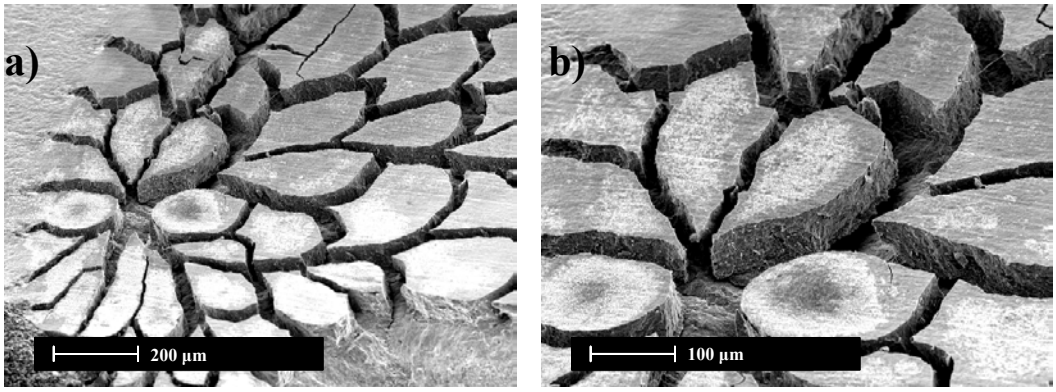

FIG. 7—*Scanning electron images of a cracked hydride blister approximately 60 μm deep and failed under equal biaxial tensile deformation at 300°C.*

As a consequence of the brittle behavior of the hydride blisters, the ductility of the Zircaloy-4 sheet is controlled by fracture of the ductile substrate beneath the cracked blister. As the substrate material strains plastically, the cracks within the blister become blunted. For hydride blisters with depths greater than about 30–40 μm, continued plastic straining initiates short cracks within the substrate at the base of blunted "blister" cracks, as shown in Fig. 8. The material continues to deform in a plastic manner accumulating strain (and strain energy density), until a crack propagates through the sheet thickness. As a result, as indicated by the failure strains in Fig. 4, tensile ductility is sensitive to crack depth, which is determined by the depth of the hydride blister. Importantly, these observations indicate that (for hydride blisters with depths >30–40 μm) the ductility of the Zircaloy is controlled by *crack growth* within the substrate beneath the cracked blister.

The nature of the crack growth process within the substrate depends on the temperature. During room temperature straining, blunted cracks within blisters with depths >30–40 μm, such as shown in Fig. 8*a*, initiate Mode I cracks within the Zircaloy substrate as fractured hydride precipitates form primary voids ahead of the crack-tip; a good example of this process is shown in Fig. 7 of Ref. [12]. Failure at room temperature eventually occurs by the growth of a mode I crack on a plane roughly *normal to the specimen surface* and therefore also normal to the maximum principal stresses in the plane of the sheet. This fracture process creates the fracture profile shown in Fig. 9*b*. Significantly, at least for the case of plane-strain tensile deformation, the failure strains can be predicted with reasonable accuracy using an elastic-plastic fracture analysis for the growth of a Mode I crack [12].

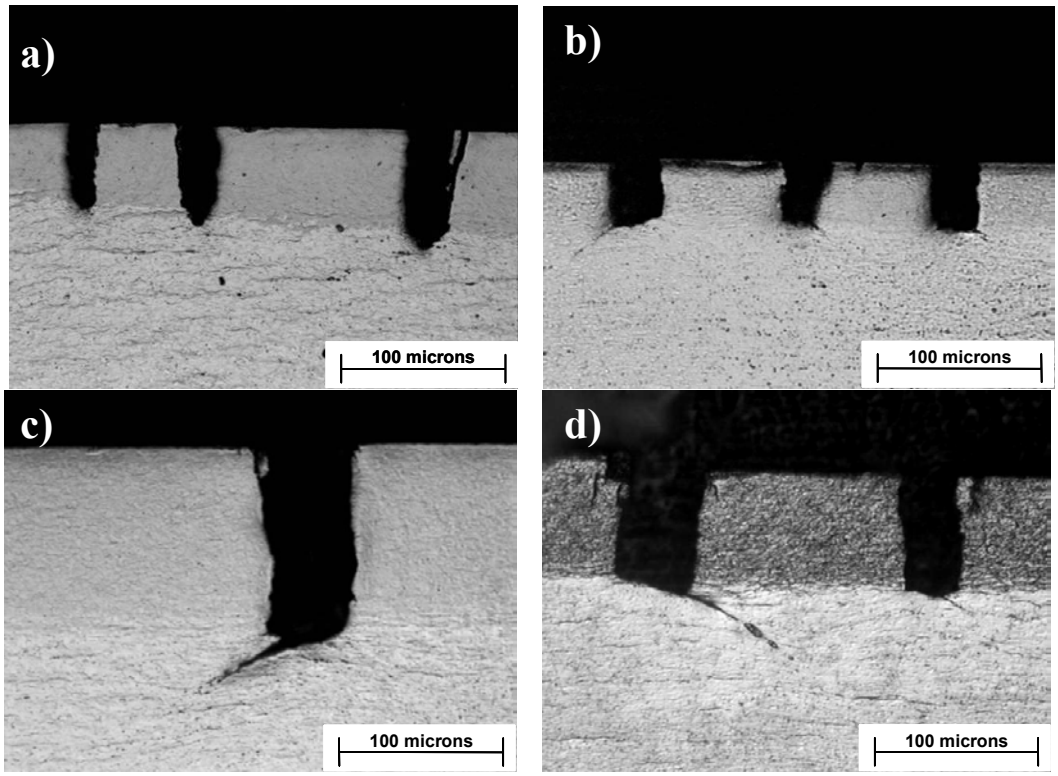

FIG. 8—*Optical micrographs showing profiles of arrested cracks beneath hydride blisters in specimens subject to equal-biaxial deformation at (a) 25°C with a blister 75 μm deep, (b) at 300°C with a blister 53 μm deep, (c) at 300°C with a blister 83 μm deep, and (d) at 375°C with a blister 84 μm deep.*

At elevated temperatures (300°C and 375°C), the hydride-blister cracks undergo extensive crack-tip blunting as the substrate deforms to higher levels than at room temperature (Fig. 4). As shown in Figs. 8*b*, 8*c*, and 8*d*, the comparative high level of deformation creates nearly flat bottom cracks that eventually initiate short mixed mode I/II cracks. The consequence is that for *all* of the hydrided Zircaloy-4 at 300° and 375° C, as well as for material with thin (<30–40 μm) blisters at room temperature (or unhydrided material), the eventual fracture plane is a macroscopic plane inclined at ≈ 45° through the thickness, as shown in Figs. 9*a*, 9*c*, and 9*d*. The pronounced crack blunting at 300°C indicates that cracks initiating within the blister are arrested by a very ductile substrate resistant to Mode I crack growth. No Mode I fracture was seen at either 300° or 375°C.

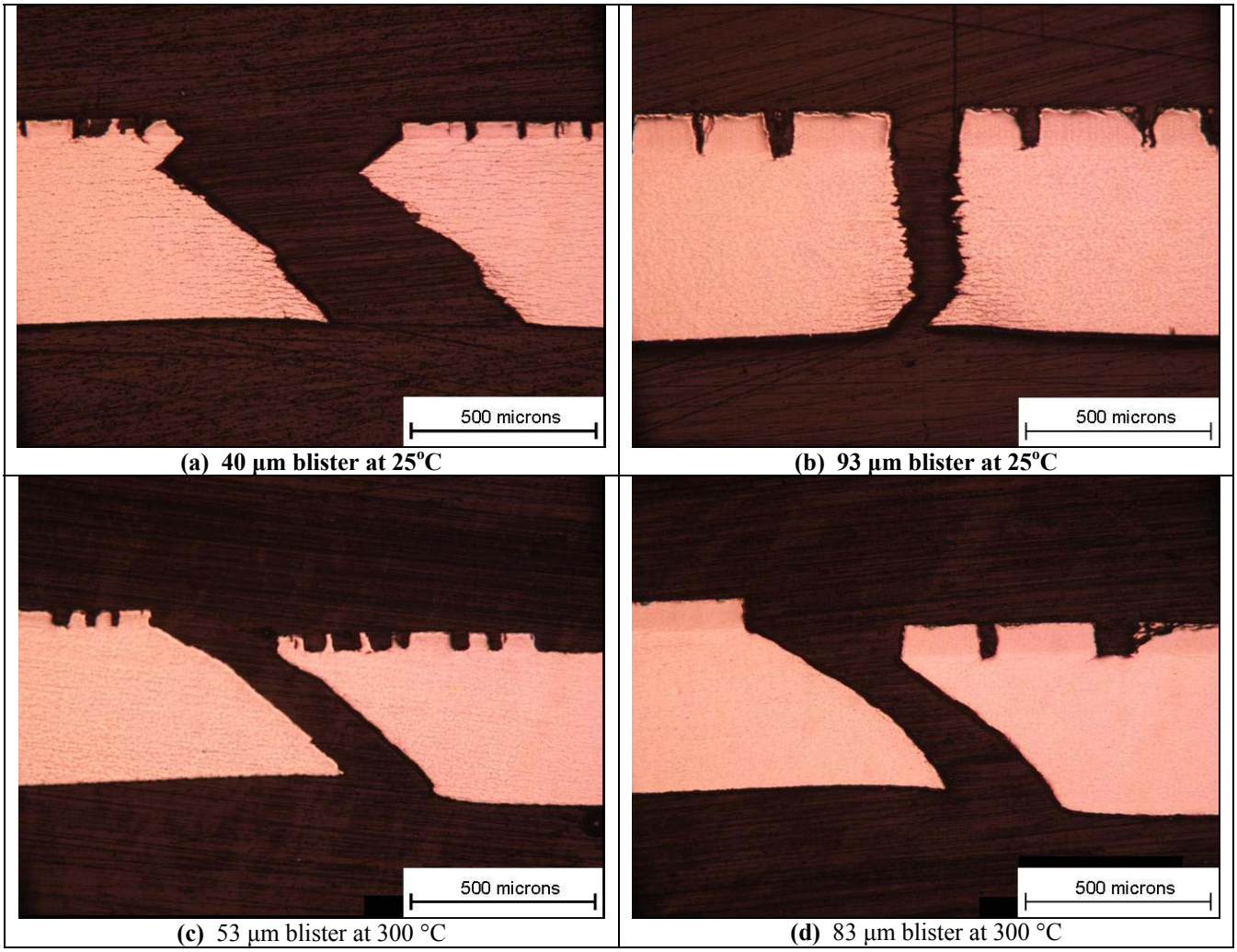

(a) 40 μm blister at 25°C **(b) 93 μm blister at 25°C**

(c) 53 μm blister at 300 °C **(d)** 83 μm blister at 300 °C

FIG. 9—*Profiles of the fracture surfaces of Zircaloy-4 containing hydride blisters and fractured under equal biaxial tensile deformation at either 25° or 300°C. Note that specimen preparation after fracture removed small sections of the hydride blister in some cases, especially on the right side of* (c).

The above observations indicate that at both 300°C and 375°C, ductility is limited by the onset of mixed Mode I/II shear crack growth through the sheet thickness. Critical to this elevated temperature failure process is the increased resistance to growth of the Mode I cracks

that initiate within the brittle blister. Material failure then eventually occurs at significantly higher levels of "ductility" (than at room temperature) by the eventual propagation of the mixed Mode I/II crack for which a high level of shear deformation is essential. This condition is known to be promoted by through-thickness plane-stress loading (i.e., plastically deforming thin sheet or cladding) in a material that is resistant to Mode I crack growth and possesses low strain and strain-rate hardening capacity. All of these conditions are met, especially at 300°C and 375°C where the ductility of the embedded hydride precipitates resists the damage accumulation necessary for Mode I crack growth [7,12,28].

These present results for the failure strains of the hydrided Zircaloy-4 sheet may be compared with the plane-strain ductility behavior of Zircaloy-4 cladding tube using a ring-stretch test procedure [11]. Based on the thickness of either the hydride blister or the rim of concentrated hydride particles, Fig. 10 shows such a comparison by normalizing the failure strains to the corresponding failure strain if no hydride blisters are present. The normalization procedure takes into account the significantly higher level of intrinsic ductility in the sheet material. From the graph it is seen that at 300°C both cladding tube and sheet follow roughly the same trend, with perhaps a greater sensitivity to hydride rim depth in the ring-stretch cladding-tube specimens. However, at 375°C, the normalized failure strains of cladding tube are considerably higher, especially at hydride rim depths of 150–200 μm. These results indicate a significant temperature effect with increased ductility at the higher temperature. Comparing failure under equal biaxial tensile deformation with that under plain-strain tension, Fig. 10 shows generally similar ductility behavior with the plane-strain case appearing slightly less ductile at 300°C. The data confirm that the equal-biaxial tensile deformation is not more penalizing to ductility than the plane-strain path.

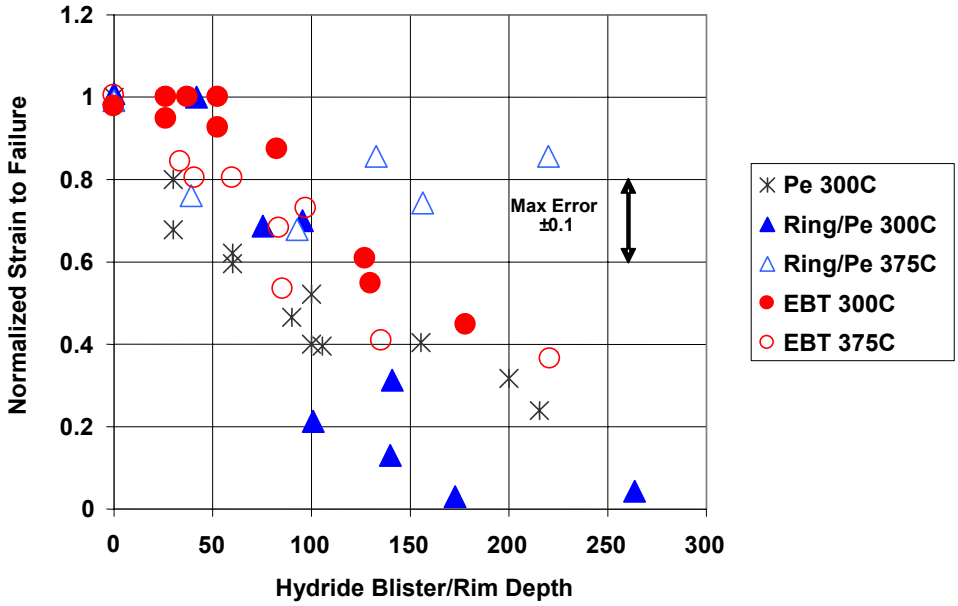

FIG. 10—*Far-field failure strains for Zircaloy-4 sheet containing hydride blisters and tested in either plane-strain tensile deformation (Pe) or equal biaxial tensile deformation (EBT) at either 300° or 375°C, normalized to the corresponding failure strain if no hydride blister is present. Also included are data for Zircaloy-4 cladding tube containing a continuous layer or "rim" of dense hydride particles. The cladding tube was tested tested under plane-strain deformation using ring stretch specimens at 300° or 375°C; the 300°C data are from Ref. [11], which also describes the corresponding hydride microstructure.*

Conclusions

Zircaloy-4 sheet containing solid hydride blisters has been fractured under equal-biaxial tensile deformation utilizing a punch-stretch test procedure at 25°, 300°, and 375°C. The resulting ductility behavior and underlying fracture process has been contrasted to that of Zircaloy-4 sheet and cladding tube containing either a hydride blister or a hydrided rim *but* subjected to plane-strain deformation. Taken as a whole, these experimental observations indicate a crack-growth fracture process that is sensitive to the presence of hydride blisters/rims in a manner that is a complex interaction among: (a) the depth of the blister/rim (which dictates the depth of the initial crack), (b) the deformation response of the substrate beneath the blister/rim, and (c) the resistance of the substrate to eventual growth of either Mode I crack or mixed Mode I/II crack. Thus, the ductility of hydrided Zircaloy in the range of plane-strain to equal-biaxial tensile deformation may be understood as follows:

1. Failure occurs as a result of a strain-driven process in which the brittle hydride blister initiates Mode I cracks (to a depth equal to that of the blister) at roughly the yield strain of the ductile substrate beneath the blister. Subsequent deformation causes crack-tip blunting, the extent of which increases at elevated temperatures. At room temperature, blunted cracks within blisters with depths ≥ 30–40 μm initiate short Mode I cracks within the substrate beneath the blister, and one of these cracks subsequently propagates as the material fractures on planes normal to the sheet surface. At elevated temperatures (300°C and 375°C), increased resistance to Mode I crack growth within the substrate causes extensive blunting of the hydride/blister cracks. As the strain increases, the highly blunted "blister" cracks eventually initiate mixed mode I/II cracks that subsequently propagate to cause fracture on a plane inclined roughly 45° to the surface.
2. The increased resistance to Mode I crack growth at elevated temperature results in a marked sensitivity of ductility to temperature such that hydrided Zircaloy-4 sheet and cladding tube is significantly more ductile at elevated temperatures (300° and 375°C) when compared to room temperature, as seen in Figs. 4 and 5.
3. The observed failure strains decrease with increased depth of the hydride blister/rim, as expected from a crack growth process. The crack-growth failure process appears to be driven by the maximum principal strain such that the failure strains in equal-biaxial tension are similar to those in plane-strain tensile deformation. Thus, at least for the hydrogen levels within the substrate in this study, the strain path has relatively little influence on ductility at a given hydride blister depth in the range between plane-strain and equal-biaxial tensile deformation.

Acknowledgments

The authors would like to thank T. Foecke of NIST for valuable advice on testing procedure and K. S. Chan of Southwest Research Institute for several useful discussions. This research was supported by the FERMI consortium at Penn State University and by Argonne National Laboratory.

References

[1] Garde, A. M., Smith, G. P., and Pirek, R. C., "Effects of Hydride Precipitate Localization and Neutron Fluence on the Ductility of Irradiated Zircaloy-4," *11th International Symposium on Zr in the Nuclear Industry, ASTM STP 1295*, Garmisch-Partenkirchen, ASTM International, West Conshohocken, PA, 1996, pp. 407–430.

[2] Meyer, R. O., McCardell, R. K., Chung, H. M., Diamond, D. J., and Scott, H. H., "A Regulatory Assessment of Test Data for Reactivity Initiated Accidents," *Nuclear Safety*, Vol. 37, 1996, pp. 872–387.

[3] Boyack, B. E., Motta, A. T., Peddicord, K. L., Alexander, C. A., Deveney, R. C., Dunn, B. M., et al., "Phenomena Identification and Ranking Tables (PIRTs) for Reactivity Initiated Accidents in Pressurized Water Reactors Containing High Burnup Fuel," *Nuclear Regulatory Commission NUREG/CR-6742*, 2001.

[4] Huang, F. H., *Fracture Properties of Irradiated Alloys*, United States: Avante Publishing, 1995.

[5] Byun, T. S. and Farrel, K., "Irradiation Hardening Behavior of Polycrystalline Metals after Low Temperature Irradiation," *Journal of Nuclear Materials*, Vol. 326, 2004, pp. 86–96.

[6] Prat, F., Grange, M., Besson, J., and Andrieu, E., "Behavior and Rupture of Hydrided Zircaloy-4 Tubes and Sheets," *Metallurgical Transactions A*, Vol. 29A, 1998, pp. 1643–1651.

[7] Arsene, S., Bai, J. B., and Bombard, P., "Hydride Embrittlement and Irradiation Effects on the Hoop Mechanical Properties of Pressurized Water and Boiling-Water Reactor Zircaloy Cladding Tubes," *Metallurgical and Materials Transactions A*, Vol. 34A, 2003, pp. 553-588.

[8] Grange, M., Besson, J., and Andrieu, E., "Anisotropic Behavior and Rupture of Hydrided Zircaloy-4 Sheets," *Metallurgical and Materials Transactions A*, Vol. 31A, 2000, pp. 679–690.

[9] Grigoriev, V., Josefsson, B., and Rosborg, B., "Fracture Toughness of Zircaloy Cladding Tubes," *11th ASTM International Symposium on Zr in the Nuclear Industry, ASTM STP 1295*, Garmisch-Partenkirchen, Germany, 1996, pp. 431–447.

[10] Yamanaka, S., Kuroda, M., Setoyama, D., Uno, M., Takeda, K., Anada, H., et al. "Analysis of the Fracture Behavior of Hydrided Cladding Tube at Elevated Temperatures by Fracture Mechanics," *Journal of Alloys and Compounds*, Vols. 330–332, 2002, pp. 400–403.

[11] Daum, R. S., Majumdar, S., Tsai, H. C., Billone, M. C., Bates, D. W., Koss, D. A., et al. "Embrittlement of Hydrided Zircaloy-4 under RIA-like Conditions," *13th ASTM International Symposium on Zr in the Nuclear Industry, ASTM STP 1423*, Annecy, France, 2002, pp. 702–719.

[12] Pierron, O.N., Koss, D. A., Motta, A. T., and Chan, K. S., "The Influence of Hydride Blisters on the Fracture of Zircaloy-4," *Journal of Nuclear Materials*, Vol. 322, 2003, pp. 21–35.

[13] Yunchang, F. and Koss, D. A., "The Influence of Multiaxial Stress States on the Hydrogen Embrittlement of Zirconium Alloy Sheet," *Metallurgical Transactions A*, Vol. 16A, 1985, pp. 675–681.

[14] Natatsuka, M., Une, K., Tokunaga, K., and Ohta, T. "Mechanical Properties of High Burnup BWR Fuel Cladding Tubes under Simulated RIA Conditions," *Proc. 2004 Int. Meeting on LWR Fuel Performance*, Orlando, FL, 2004, pp. 526–535.

[15] Kearns, J. J. and Woods, C. R., "Effect of Texture, Grain Size, and Cold Work on the Precipitation of Oriented Hydrides in Zircaloy Tubing and Plate," *J. Nucl. Mater.*, Vol. 20, 1966, pp. 241.
[16] Delobelle, P., Robinet P., Bouffioux, P., Greyer, P., and LePichon, I., "A Unified Model to Describe the Anisotropic Viscoplastic Zircaloy-4 Cladding Tubes," *11th International Symposium on Zr in the Nuclear Industry, ASTM STP 1295*, Garmisch-Partenkirchen, 1996, pp. 373–393.
[17] Tenckhoff, E., "Deformation Mechanisms, Texture and Anisotropy in Zirconium and Zirconium Alloys," *ASTM STP 966*, ASTM International, West Conshohocken, PA, 1988.
[18] Pierron, O. N., Koss, D. A., and Motta, A. T., "Tensile Specimen Geometry and the Constitutive Behavior of Zircaloy 4," *Journal of Nuclear Materials*, Vol. 312, 2002, pp. 257–261.
[19] Link, T. M., Koss D. A., and Motta, A. T. "Failure of Zircaloy Cladding under Transverse Plane-Strain Deformation," *Nuclear Engineering and Design*, Vol. 186, 1998; pp. 379–394.
[20] SCDAP/RELAP5/MOD2, *Code Manual Volume 4: MATPRO: "A Library of Materials Properties for Light Water Reactors Accident Analysis," NUREG/CR-5273, EG-2555, chapter 4.9.*, 1990.
[21] Marciniak Z. and Kuczynski, K., "Limit Strains in the Process of Stretch-Forming Sheet Metal," *International Journal of Mechanical Sciences*, Vol. 9, 1967, pp. 609–620.
[22] Raghavan, K. S., "A Simple Technique to Generate In-Plane Forming Limit Curves and Selected Applications," *Metallurgical and Materials Transactions A*, Vol. 26A, 1995, p. 2075–2084.
[23] Marciniak, Z. and Duncan, J., *Mechanics of Sheet Metal Forming*, London, E. Arnold, 1992.
[24] Efsing, P. and Pettersson, K., "The Influence of Temperature and Yield Strength on Delayed Hydride Cracking in Hydrided Zircaloy 2," *Zirconium in the Nuclear Industry, 11th International Symposium, ASTM STP 1295*, ASTM International, West Conshohocken, PA, 1996, pp. 394–404.
[25] Huang, J. H. and Ho, C. S., "Subcritical Crack Growth Behavior for Hydrided Zircaloy-4 Plate," *Materials Chemistry and Physics*, Vol. 47, 1997, pp. 184–192.
[26] Daum, R. S., Majumdar, S., Tsai, H., Bray, T. S., Koss, D. A., Motta, A. T. et al., "Mechanical Property Testing of Irradiated Zircaloy Cladding Under Reactor Transient Conditions," *Proc. 4th Int. Sym. on Small Specimen Test Techniques, ASTM STP 1418*, ASTM International, West Conshohocken, PA, 2002, pp. 195–210.
[27] Nagase, F. and Uetsuka H., "Hydride Morphology and Hydrogen Embrittlement of Zircaloy Fuel Cladding Used in NSRR/HBO Experiment," P*roceedings of the ANS International Topical Meeting on Light Water Reactor Performance, ANS*, Portland, OR, 1997, p. 677.
[28] Bai, J. B., Prioul, C., and Francois D., "Hydride Embrittlement in Zircaloy-4 Plate: Part I. Influence of Microstructure on the Hydride Embrittlement in Zircaloy-4 at 20° and 350°C," *Metallurgical and Materials Transactions A*, Vol. 25A, 1994, pp. 1185–1197.